**Figure 7.** Diagram of serological relationships of viral and cellular DNA polymerases.[19] TDSNV, Trager duck spleen necrosis virus; REV-T, reticuloendotheliosis virus (strain T); CSV, chick syncytial virus.

duck spleen necrosis virus DNA polymerase. The specificity of these neutralization reactions was shown by the ability of the reticuloendotheliosis virus (strain T) DNA polymerase and the Trager duck spleen necrosis virus DNA polymerase to block the activity of the antibodies used in Figure 6 against their homologous DNA polymerases.

Further evidence for serological relationships among the DNA polymerases of the reticuloendotheliosis viruses, the avian leukosis-sarcoma viruses, and the normal chicken cell was the ability of the chicken cell 10S DNA polymerase and the Rous sarcoma virus–Rous associated virus-0 DNA polymerase to block the neutralizing activity of antibody to Trager duck spleen necrosis virus DNA polymerase against the Trager duck spleen necrosis virus DNA polymerase.

These serological relationships were about 100-fold weaker than those of viruses in the same group. These weak serological relationships only appeared after partial purification of the DNA polymerases, perhaps as a result of conformational changes of the DNA polymerases during purification.

These serological relationships are diagrammed in Figure 7. There are serological relationships between the DNA polymerases of chicken cells and reticuloendotheliosis viruses, and there are serological relationships between the DNA polymerases of the reticuloendotheliosis viruses and the avian leukosis-sarcoma viruses. Serological relationships were also found between the DNA polymerases of the avian leukosis-sarcoma viruses and the chicken cell.[19]

These serological relationships among the DNA polymerases of the normal chicken cell and of these avian RNA viruses indicate that these DNA polymerases probably have amino acid sequence homology. This homology indicates a common evolutionary origin from an ancestor DNA polymerase. This homology supports the hypothesis that these viruses originated from normal cell components. Some of the amino acid sequences of the original DNA polymerases may have been conserved in the evolution leading to the formation of these RNA viruses, and these sequences might have given rise to the observed serological relationships.[20]

## Summary

In this Account, I have described some biochemical characteristics of RNA-directed DNA polymerase activity and its distribution and possible role in some biological systems. In addition, I have presented evidence supporting the hypothesis that the viruses whose virions contain RNA and a DNA polymerase evolved from normal cell components.

(20) H. M. Temin, *Annu. Rev. Genetics*, in press.

# On the Aggregation of Dissolved Alkane Chain Molecules

George W. Brady

*Bell Laboratories, Murray Hill, New Jersey 07974*

The aggregation of chain-like molecules is a fascinating phenomenon; it is of importance in such areas as liquid crystals[1,2] and micelle formation in soaps and detergents,[3-5] and in biological membrane phenomena.[6] From an X-ray diffraction viewpoint, with the exception of the soap studies, no concerted attack on the problem has been made, primarily because of the difficulty in measuring the low intensities characteristic of liquid scattering. With respect to micelles we note the early work of Harkins and collaborators[4] and Philipoff[5] and the culmination of this effort in the classic work of Luzzatti[3] where the basic concepts of micelle formation were clarified.

As far as simple-chain alkanes are concerned, measurements were made many years ago by Stewart and coworkers,[7] and some interpretive work on

George W. Brady received his Ph.D. in Physical Chemistry at McGill University, where he was a National Research Council of Canada Fellow. He was subsequently a research associate at the University of Chicago and a research fellow at Harvard University before joining the technical staff at Bell Laboratories. His interest there has been in liquid diffraction. His work includes studies on ionic solution structure, critical phenomena, phase transformations, liquid crystals, and aggregation and interaction of large molecules.

(1) A. DeVries, *Mol. Cryst. Liquid Cryst.*, 10, 219 (1970); 11, 361 (1970).
(2) G. W. Brady, *J. Chem. Phys.*, 57, 91 (1972); G. W. Brady, C. Cohen-Addad, and E. F. X. Lyden, *J. Chem. Phys.*, 51, 4309 (1969).
(3) H. F. Reiss and V. Luzzatti, *J. Colloid Interface Sci.*, 21, 534 (1966).
(4) W. D. Harkins, "The Physical Chemistry of Surface Films," Reinhold, New York, N. Y. 1952.
(5) W. Philipoff, *Discuss. Faraday Soc.*, 11, 96 (1951).
(6) A. R. Oseroff, P. W. Robbin, and M. M. Borger, *Annu. Rev. Biochem.*, 42, 835 (1973).

the Stewart data was undertaken by Warren.[8] Stewart and Warren were concerned with the measurement and elucidation of diffraction peaks that were characteristic of spacings much greater than those attributable to atomic nearest neighbors. In fact, they found that these spacings were related to the chain lengths in some way, although a rigorous relation was never derived. For example, Stewart postulated that cybotatic groupings of molecules were responsible for the diffraction effects. Warren,[8] noting that the peaks were enhanced when one end of the chain contained a polar group, interpreted the data as arising from a scattering between an excess electron density at that end of the molecule and a deficit at the other.

Some years ago we began experiments[2,9,10] on solutions of large organic molecules, using a heavy atom substitution technique. By this means, the scattering power of one part of a large molecule was preferentially increased so that structural features arising from interactions of that part with some other molecule could be identified.[10] Kratky and coworkers[11] also applied a variation of this method to some simple molecules. Using this technique we found that in solutions of alkanes terminally singly substituted by halogens[2,10] the X-ray intensity patterns exhibited peaks corresponding to an interhalogen distance roughly equivalent to that of the doubly terminally substituted chain of twice the number of carbons. Since the terminal alkane ends should have no influence in bringing about such an ordering, and since it is obviously the highly polarizable atoms that tend to make maximum contact with each other, a configuration of only two molecules is ruled out. The indication is that ordered aggregates of solute molecules are present.

It is to elucidate this aggregation phenomenon that we address ourselves in this Account. The effects to be reported here have all been observed with decalin, a nonflexible, nearly spherical molecule, as solvent. They are *not* observed when a chain molecule similar to the solute is the solvent. The reader is referred to the references cited in the text for experimental details, particularly references 2, 10, and 12. We only mention that the intensities are low and must be measured with monochromatic radiation under vacuum or in a helium atmosphere, to remove air scattering.

The theory, as detailed in ref 10 and 13, follows quite directly from the equation for a system of two types of scatterer. For this system the intensity in electron units[2] is given by

$$I = x_a f_a{}^2[1 + x_a A] +$$
$$(1 - x_a)f_b{}^2[1 + (1 - x_a)B] + 2x_a(1 - x_a)f_a f_b D \quad (1)$$

where $A$, $B$ and $D$ are correlation integrals of the form

(7) G. W. Stewart and R. M. Morrow, *Phys. Rev.*, **30**, 232 (1927); **31**, 174 (1928).

(8) R. E. Warren, *Phys. Rev.*, **44**, 969 (1933).

(9) G. W. Brady, *J. Chem. Phys.*, **32**, 45 (1960).

(10) G. W. Brady, E. Wasserman, and J. Wellendorf, *J. Chem. Phys.*, **47**, 855 (1967).

(11) O. Kratky and W. Worthmann, *Monatsh. Chem.*, **76**, 263 (1947); O, Kratky, G. Porod, and A. Sekora, *ibid.*, **78**, 295 (1948).

(12) G. W. Brady and M. L. Kaplan, *J. Chem. Phys.*, **58**, 3535 (1973).

(13) B. E. Warren, "X-Ray Diffraction," Addison-Wesley, Reading, Mass., 1969, pp 116–142.

$$4\pi\rho \int_0^\infty r^2 g_{ij}(r)\frac{\sin sr}{sr}dr$$

and $x_a$ is the mole fraction of atoms of type a. The factor $g_{ij}(r)$ is a radial distribution function, generally written as $[g_{ij}(r) - 1]$, and for $A$, $B$ and $D$, $g_{ij}$ is $g_{aa}$, $g_{bb}$, and $g_{ab}$, where the subscripts indicate that the correlation is for the a atoms with themselves, the b atoms with themselves, and the a and b atoms with each other, respectively. The radial distribution function is defined to mean that $4\pi r^2\rho g_{aa}dr$, for example, gives the number of a's in a spherical shell of radius $r$ and thickness $dr$ about each a; $g_{bb}$ and $g_{ab}$ are similarly defined. Finally, $\rho$ is the mean number of atoms per cubic ångström, $f_a$ and $f_b$ are the scattering factors of the a and b atoms, and $s = (4\pi/\lambda)\sin\theta$, where $2\theta$ is the scattering angle.

Equation 1 applies to a system in which the correlations are not independent, in the sense that the sum of the coefficients of the $A$, $B$, and $D$ terms is unity. As will be seen, this condition does not hold in our experiment, and the equation will have to be modified.

## Results and Discussion

Figures 1 and 2[12] show scattering curves for solutions of chains of different lengths. Figure 1 is for equimolar (5 mol %) concentrations of terminally substituted monoiodides of chain lengths $C_m$ and $C_n$, where $m$ and $n$ refer to the number of carbon atoms. The sum $m + n = 22$ is constant in all the systems, while the ratio $m/n$ varies from 0.83 to 0.1. The curves of Figure 2 are for fixed total concentrations of $C_{20}$ and $C_2$ chains. These lengths are prototypes for a long ($C_L$) and a short ($C_S$) chain, respectively. Curve 1 is for a system of $C_L$'s only. Successive fractions of $C_L$'s have been replaced by $C_S$'s in curves 2, 3, and 4; in curve 4 all the $C_L$'s have been replaced.

The results are striking. In the $C_{10}$–$C_{12}$ curve of Figure 1, there is a single peak at $s \sim 0.32$ Å$^{-1}$ which corresponds to a mean distance of $\sim24$ Å,
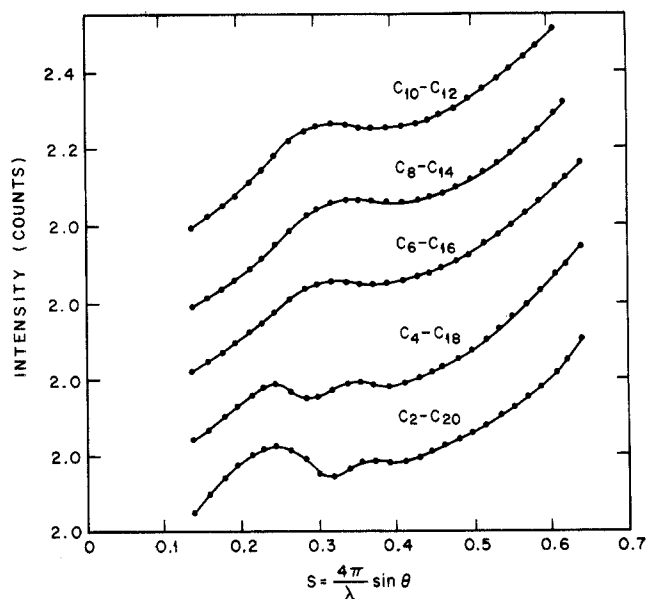


**Figure 1.** Intensity patterns of a set of solutions of different chain lengths. The sum of the carbon atoms on the two chains always equals 22.
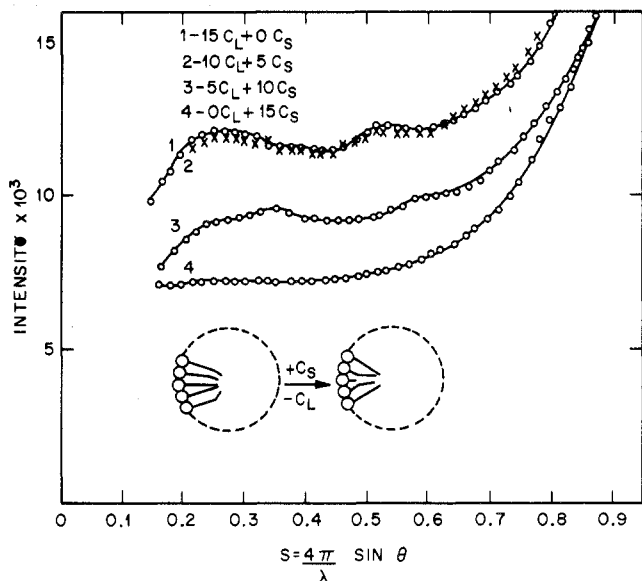
**Figure 2.** Intensity patterns of $C_L + C_S$ solutions. The total number, $C_L + C_S = 15$ per 100 molecules of solution, is constant, while the composition varies from all $C_L$ to all $C_S$.
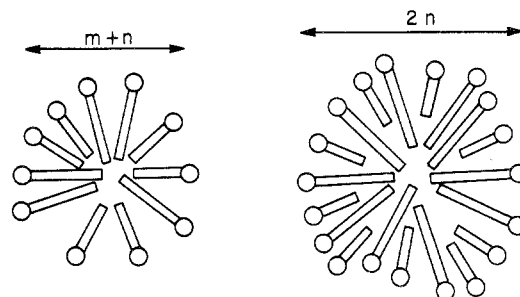


**Figure 3.** Schematic of the aggregation of dissolved chain molecules. At the left the disparity in length is not great, whereas at the right it is. The shorter molecules occupy positions at the periphery. The solvent is decalin ($C_{10}H_{18}$).
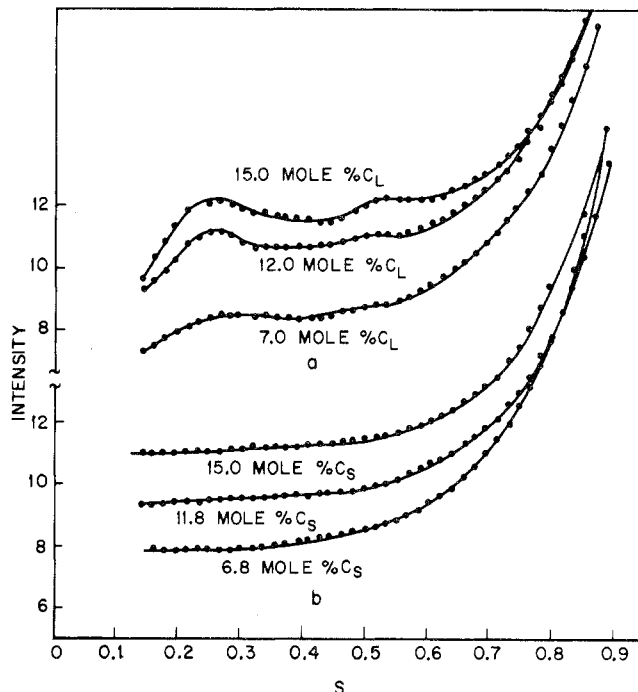


**Figure 4.** Intensity patterns of solutions of long ($C_L$) and short ($C_S$) chains at different concentrations.

close to the sum of the two chain lengths. As $m/n$ decreases the peak intensity also decreases, and another one grows in at $s \sim 0.24$ Å$^{-1}$. For the $C_2$-$C_{20}$ solution this latter peak is dominant and the $s \sim 0.32$ Å$^{-1}$ one has nearly disappeared. The $s \sim 0.24$ Å$^{-1}$ peak corresponds to a distance of $\sim 38$ Å, roughly equivalent to twice the length of the longest of the two chains.

These observations lead to a preliminary model shown in Figure 3. The molecules are pictured as forming an aggregate in which their end groups are arrayed on the surface of a sphere (the actual shape determination is discussed later). For chains of not too dissimilar lengths, the diameter is given by the sum of the individual chain lengths, as sketched at the left. When the length disparity becomes large, as shown at the right, the diameter is determined by the length of the longer molecule; the shorter molecules interleave with the longer ones so that their end groups also lie on the periphery. This disposition for the short chains follows from the findings that the total intensity for the two structures is the same. The short chains must therefore be contributing, and the distance between their ends must be equivalent to that between two longer chains. This assignment of $C_S$ in the mixed aggregate is confirmed by curves 1 and 2 of Figure 2, which shows that a significant fraction, in this case one-third, of the long chains can be replaced by short ones without any significant change in the scattering.

Figure 2 also shows that the superstructure pattern of curve 1, for the $C_L$ chains, is completely absent in curve 4, for $C_S$ chains only, indicating that a minimum length is required to render the chains capable of aggregating into a superstructure. That this finding is independent of concentration can be seen in Figure 4 which displays curves for $C_L$ and $C_S$ chains,[12] measured at three concentrations. Indeed, as curve 4a indicates, the only effect of concentration appears to be a proportional increase in the $C_L$ superstructure intensity pattern, paralleled by a proportional increase in the background intensity on

which it sits. Similarly, the equivalent curves for the $C_S$ chains of curve 4b show the same proportional increase with iodine concentration; no new features develop in either set of curves.

With these experiments it is possible to isolate the scattering function of the aggregate. To do this we separate the intensity into its three components related to the radial distribution functions $g_{II}$, $g_{CC}$, and $g_{CI}$, respectively. We determine these terms and their coefficients from the intensity patterns of the $C_S$ solutions, where there is no superstructure component. Once these are known, the close order contributions to the intensities of the $C_L$ solutions are evaluated from them. Subtracting these out then leaves the superstructure scattering. This is equivalent to stating that the $g$'s are the same in both systems, and the justification for this procedure will become evident in the analysis; it is in fact a major finding of the work.[12]

We let a and b of eq 1 represent the iodine and carbon atoms, respectively. Since Figure 4 shows that the intensity is proportional to the mole fraction, $x$, of I atoms, eq 1 does not adequately describe the scattering. This indicates that the first term in the equation does not reflect the fact that the I's are aggregated and therefore, from a scattering view-
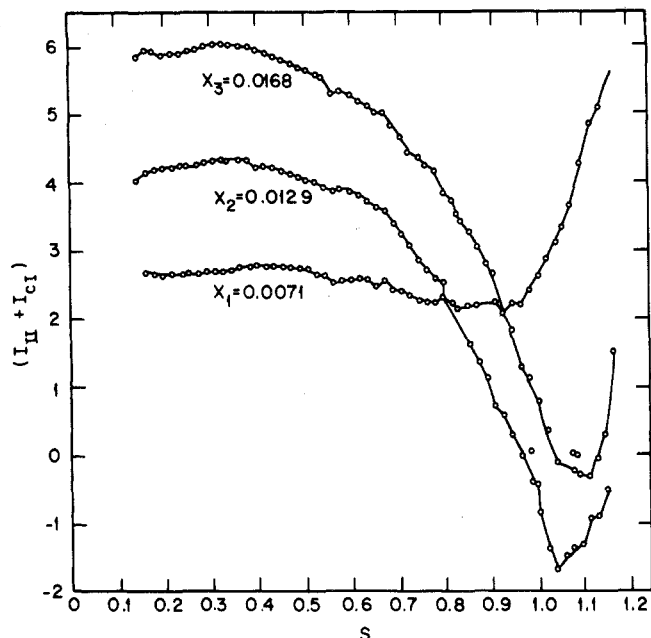
**Figure 5.** Curves for $I_{II} + I_{CI}$ obtained by subtracting the intensity pattern of an alkane solution of equivalent concentration from the curves of Figure 4b.
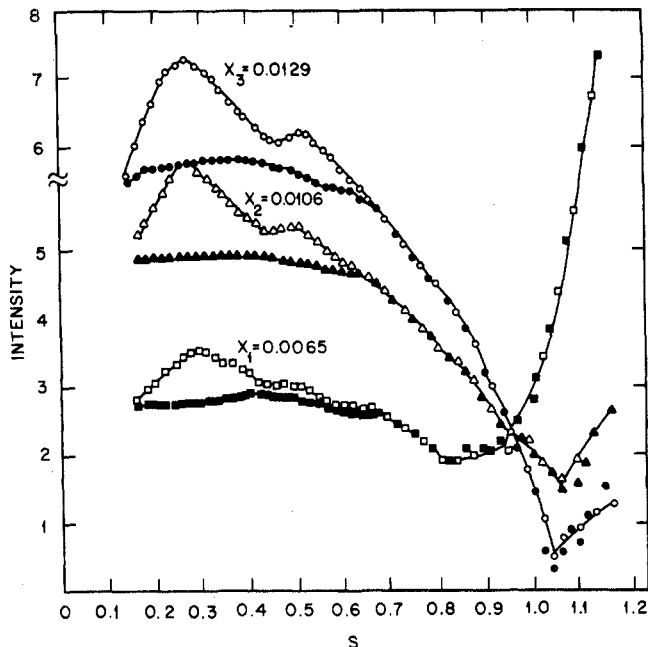


**Figure 6.** The $I_{II} + I_{CI}$ curves for the $C_L$ solutions of Figure 4a (open symbols) at the three concentrations. The close order background curves (solid symbols) are calculated using the terms obtained from the $C_S$ curves.
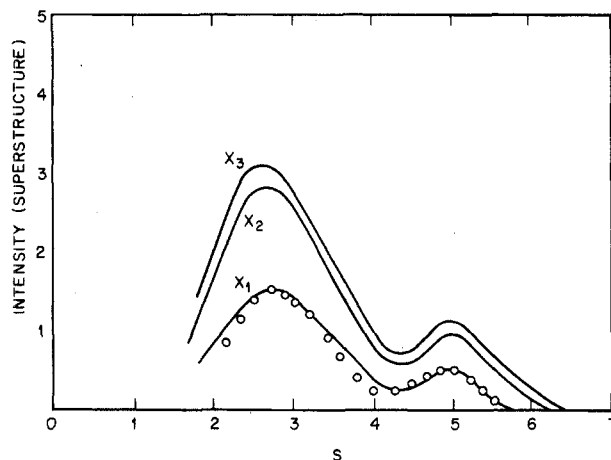


**Figure 7.** Superstructure scattering curves for the three $C_L$ concentrations. The circles show the calculated scattering curve for a hollow sphere of radius $17 \pm 1$ Å.

point, should be treated as an independent term not influenced by the other terms of the equation. This is done by setting the coefficient $x$ of the $A$ correlation term equal to unity; this is, of course, equivalent to saying that $A$ is independent of the dilution.

As previously described[2] we approximate the C–C contribution by the scattering from an alkane solution of equivalent concentration. There then remains only the coefficient of the $g_{CI}$ term to be determined. Ideally this term should disappear since we are now treating the system as two independent ones, but this is not true in this case because there are C–I correlations in individual molecules to be taken into account. We then replace $2x(1 - x)$ by $\phi(x)$ to indicate that the coefficient is undetermined, and write that

$$I = xf_i^2[1 + A] + (1 - x)I_{alkane} + \phi(x)f_If_cD$$
$$= I_{II} + I_{CC} + I_{CI} \qquad (2)$$

Subtraction of the alkane term then gives as remainder $I_R = I_{CI} + I_{II}$, and the resultant curves are shown in Figure 5. The curves show, first, an overall increase in intensity with concentration and, second, the appearance of a minimum at $s \sim 1.05$ Å$^{-1}$, which increases toward higher concentration in an apparently quadratic way. We can easily resolve the curve into its components by writing

$$I_R(x) = I_{II}(x) + I_{CI}(x)$$
$$= xI^0_{II} + x^2I^0_{CI} \qquad (3)$$

Any two of the curves of Figure 4 can now be used to evaluate $I^0_{II}$ and $I^0_{CI}$. When the values so determined are inserted back into the equation and a slight correction is applied to the $I_{CC}$ term, the experimental curves are reproduced.[12]

When we insert the values of $I^0_{II}$ and $I^0_{CI}$ for the short chains and the appropriate values of $x$ for the $C_L$ solutions into eq 3, we obtain the results shown in Figure 6 (solid symbols). The calculated and mea-

sured values for each $C_L$ concentration superimpose throughout the whole angular range, except in the region of the superstructure scattering pattern. This implies that the close order I–I and C–I structures (as mirrored by the respective $g$'s) are the same for long and short chains. The reason for this has already been discussed in the case of $g_{CI}$. For $g_{II}$ it indicates that there is an equivalent amount of I–I contacts in both types of solution. The dominant role of chain length or some property of chain length[12] in promoting superstructure thus becomes apparent; it is the only property left to explain the difference between the measured and calculated curves of Figure 6.

Figure 7 shows the shape scattering functions completely separated from the close-order scattering. We write for the superstructure another correlation function $G(r)$ defined such that $G(r)$ is the probability density of scattering material between radii $r$ and $r + dr$.[12] The amplitude of the scattering is then described by

$$A_s = \int_0^\infty 4\pi r^2 G(r) \frac{\sin sr}{sr} dr \left[ \int_0^\infty 4\pi r^2 G(r) dr \right]^{-1} \quad (4)$$

For a hollow sphere, in which the scattering matter is distributed in a shell of thickness $(1 - C)R$, where $1 > C > 0$,[2] the correlation then must satisfy the requirements that $G(r) = 1$ for $R > r > CR$ *and* $G(r) = 0$ for $r > R$ and $CR > r > 0$. After inserting these in eq 4 and integrating, the amplitude, $A_S$, becomes, for $C \to 1$

$$A_s = (\sin sR)/sR \quad (5)$$

The scattering $I_S$ is given by $A_S^2$. The open circles in Figure 7 show the function plotted for $R = 17.0 \pm 1.0$ Å. The agreement is very good.

Returning to length considerations, Figure 8 shows X-ray patterns of a series of chains whose length varies between $C_2$ and $C_{20}$.[14] The curves are actually $I_{CC} + I_S$, obtained by subtracting out the $I^0{}_{II}$ and $I^0{}_{CI}$ contributions, previously derived, from the measured curves. The first three curves, for the $C_2$, $C_4$, and $C_6$ chains, show a slight change in slope, but are otherwise featureless. The curve for the $C_8$ chains, however, signals an abrupt change, with the appearance of the characteristic double peak superstructure pattern. The curves for the $C_{10}$ and $C_{20}$ chains show the same features, the peaks moving to lower values of $s$ as the chains lengthen from $C_8$ to $C_{20}$. When the superstructure patterns are isolated by subtracting out the $I_{CC}$ component it is found that the aggregate radii are 10.0, 12.4, and 17 Å for the $C_8$, $C_{10}$ and $C_{20}$ curves, values in agreement with the equivalent perturbed chain lengths.[2] The integrated intensity per unit mole fraction of iodine is the same for the $C_{10}$ and $C_{20}$ chains, showing that the aggregation is complete for chains of ten atoms or greater. For $C_8$, curve 1 it is about 80% of that of curves 1 and 2, indicating that the transition, though sharp, is not discontinuous.

The cooperative effect of the chain interaction is thus established by the experiments. Quite evidently the fact that $g_{II}(r)$ is independent of chain length is an important one in the phenomenology of the process for it implies that the nearest neighbor environment of the iodines does not change with aggregation. This indicates that the I end of the chain, where the molecules are primarily held together, acts as a pivot point for the process. This is illustrated schematically in Figure 9. The aggregation can then be pictured as a swivelling action around the I–I point of contact so that the chains are brought into maximum attractive contact with each other. Addition of extra links to the chains thus increases the attraction not only because of the greater number of attracting units in the chain but also because of the increased flexibility brought about by the increased possibility for trans–gauche rotation[15] about the C–C bonds.

Aggregation of the short chains is hindered by an unfavorable ratio of head-group area relative to chain length (Figure 9). The aggregate radius is determined by the length, and for a short chain like $C_2$–I, for example, of length $\sim 5$ Å, only eight molecules can be accommodated in a spherical aggregate
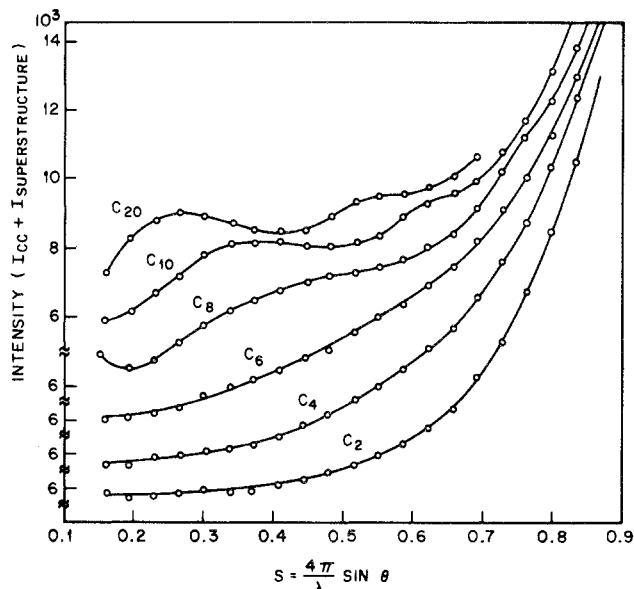


Figure 8. The curves $I_S + I_{CC}$ of the set of solutions of different chain lengths, as indicated on the curves.
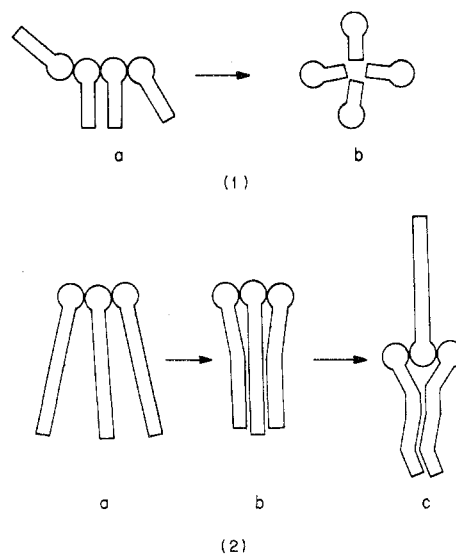


Figure 9. Two-dimensional sketch of the aggregation process. Only a few chains are shown. Parts 1a and 1b show that short chains cannot aggregate without moving the head groups apart, thus hindering the swivel action. Part 2 shows how the rotational isomerism of the segments of the long chains increases the interchain attraction (2b); at the same time the finite chain width could cause a large hole to form in the center (2b). This is overcome by rotating some chains outward (2c).

of this size, and we would have to assume an unrealistic value of 40 Å$^2$ for the cross-sectional area of the terminal I groups to satisfy the criterion that they be in contact on the surface. This constraint becomes less with increasing chain length because of the smaller surface-to-volume ratio of the aggregate. At the $C_8$–I chain length, the one where superstructure first appears, the geometry is no longer unfavorable, and a simple calculation gives 27.3 Å$^2$ for the area of the terminal group.[15] This leads to a value of 2.8 Å for the radius when hexagonal packing on the aggregate surface is assumed. Measurements on molecular models, with the group in trans and gauche positions, show this to be a reasonable value.[15]

The aggregate radius is determined by the per-

(14) G. W. Brady, *J. Chem. Phys.*, **58**, 3542 (1973).

(15) W. J. Leonard, R. L. Jernigan, and P. J. Flory, *J. Chem. Phys.*, **43**, 2256 (1965).
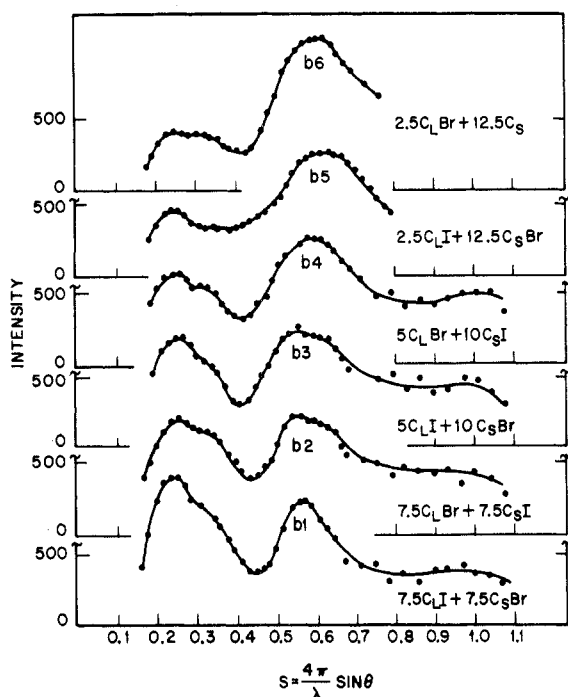
**Figure 10.** Isolated superstructure patterns of solutions containing an excess of short chains. The modulation produced by alternating the labels on the long and short chains is clearly evident.



**Figure 11.** Graphical representation of the successive removal of the different components of the scattering of curve b1 of Figure 10. The components identified on curves 1, 2, and 3 are the long-chain component, the correlation term, and the short-chain component.

turbed chain length and not the fully extended one. The mean end-to-end distance increases as $n^{1/2}$ ($n$ is the number of bonds), while the volume increases as $n$, because of the finite width of the chain. As the chains lengthen, the excess volume so engendered cannot be accommodated in the aggregate. Therefore, some of the molecules are constrained to rotate outwards from the main body of the aggregate. This is shown in configuration 2c. The volume available to each molecule in the interior is then increased. We can estimate the relative numbers of chains pointing outwards. For the $C_{10}$ and 1933 $Å^2$ for the volume and surface, respectively, the volume of the molecule is 189 $Å^3$,[15] and therefore the number of molecules pointing into the aggregate is ~66. With the value of 27.3 $Å^2$ for the effective end group area we arrive at the figure of ~71 for the number of molecules on the surface, the five extra molecules, with the total volume 945 $Å^3$, having been rotated out of the interior, leaving the remainder free to assume the conformation appropriate to maximum interchain contact. The comparable figures for the $C_{20}$ aggregate are 86 for the interior and 133 for the surface; that is, a fraction 0.342 of the chains point outwards. This is identified with (and is a more accurate determination of) the fraction 0.333 of $C_S$ chains replacing $C_L$ chains determined from the experiments of Figure 2.

Figure 10 shows a final set of intensity curves for systems in which the concentration of short chains is equal to or in excess of that of the long chains.[16] In these experiments, I and Br labels are alternately used on the long and short chains so that at each concentration it is possible to follow the placement of each chain in the aggregate scheme from the modulation in intensity produced by the difference in scattering power of the two labels.

The most striking feature of the curves is the appearance of another double peak scattering function,

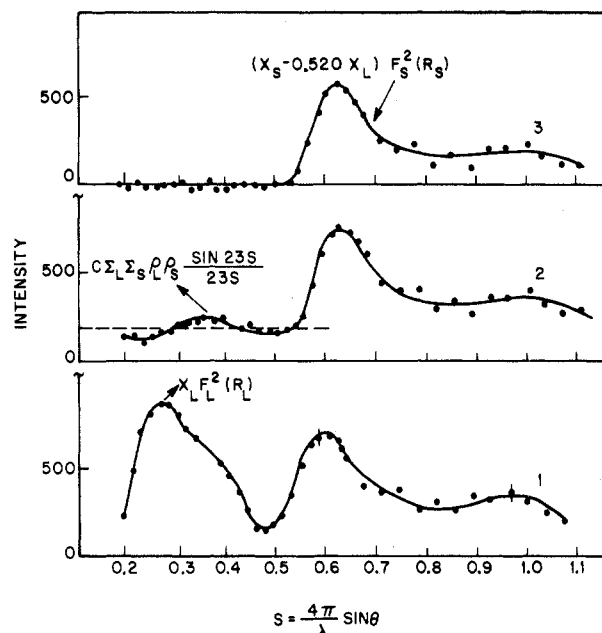(16) G. W. Brady, *J. Chem. Phys.*, in press.

whose primary maximum occurs at $s \sim 0.6$ $Å^{-1}$. This scattered intensity is completely absent in the systems composed solely of long or short chains (curves 1 and 4, Figure 2). Its features are similar to those of the superstructure pattern of the long chains and implies an aggregation of the same type, but involving the short chains, consistent with the shift toward higher $s$. The corresponding radius is 7.3 $Å$. Its area does not modulate as expected when a Br and an I are exchanged on the short chain, suggesting that the head groups of both long and short chains contribute to the scattering. Associated with the appearance of the new scattering pattern is a peak at $s \approx 0.36$ $Å^{-1}$, indicating a correlation at 23 $Å$; the long- and short-chain aggregates appear to be joined together, since the 23-$Å$ correlation can be identified with the distance between the centers of the long and short chain subunits, when mutual interpenetrability of their surface is allowed for.

Since the extra scattering only appears after a fraction, 0.342, of the short chains has been incorporated into the existing long-chain aggregates, the remaining short chains seem to coalesce into aggregates on the surface of the long-chain entities and remain attached to them. To confirm this qualitative picture we will separate the curves into their respective components and evaluate each quantitatively. We illustrate the calculation graphically in Figure 11 for curve b1 of Figure 10. The contribution $I_{S(L)}$ of the $C_L$ aggregate is given by[16]

$$I_{S(L)} = x_L[f_L{}^2 + 0.342f_S{}^2 + 0.117(f_S{}^2 - f_L{}^2)I_S \qquad (6)$$

where $x_L$ is the mole fraction of $C_L$ chains, $f_L$ and $f_S$ are the scattering factors of the long- and short-chain label atoms, and $I_S$ is the superstructure pattern for a system of I labeled long chains (Figure 7). Removing this contribution from curve 1 isolates the peak at $s \approx 0.36$ $Å^{-1}$ and identifies it as the maximum of a sinusoidal function; this is seen on the left of curve

2. The correlation associated with this function must be that between the negative densities $-\rho_L$ and $-\rho_S$ found at the respective centers of the joined long- and short-chain aggregates.

To evaluate its intensity we expand the Debye[17] equation into the form

$$I_C = \rho_L{}^2 + n\rho_L{}^2 + 2n\rho_L\rho_S(\sin sR_{LS})/sR_{LS} \qquad (7)$$

where $n$ is the number of short-chain aggregates associated with each long-chain aggregate; it can be determined from the concentration and radii of the aggregate.[16] We can estimate $-\rho_L$ and $-\rho_S$ from the electron densities of the spherical shells of the aggregates. Equation 7 can be tested quantitatively by inserting the values of $-\rho_L$, $-\rho_S$, and $n$ and subtracting it from curve 2 to obtain curve 3. As the result shows, 6 and 7 account for all the intensity but that attributable to the structure assumed by the excess short chains.

The function so isolated in curve 3 can now be evaluated. The intensity $I_{S(S)}$ can be derived in a manner analogous to that used for $I_{S(L)}$. The resulting expression is

$$I_{S(S)} = [x_S - 0.520x_L][f_S{}^2 + (N/n_S)(0.658f_L{}^2 +$$
$$0.342f_S{}^2) + 0.658(N/n_S)^2(f_L - f_S)^2][(\sin sR_S)/sR_S]^2 \quad (8)$$

where $n_S$ is the number of chains in a $C_L$ aggregate and $N$ is the number of long-chain end groups shared by the $C_S$ aggregate. This important number can thus be obtained from the measured areas of the isolated curves. The values of $N$ determined in this way are, for the six systems of Figure 10, 6.2, 5.8, 6.0, 6.0, 6.5, and 5.5, respectively. The similarity and magni-

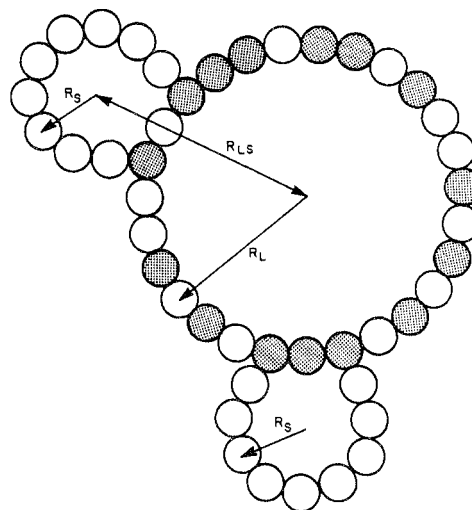(17) P. Debye, *Ann. Phys. (Leipzig)*, **46**, 809 (1915).



**Figure 12.** Two-dimensional representation of the pattern formed by the high scattering atoms in the combined aggregate. The shaded circles are the long chain end atoms.

tude, ~6, of the values indicate a significant and like amount of shared surface atoms, consistent with the observed low value of the distance $R_{LS}$ between the centers.

A two-dimensional representation of the aggregate structure is shown in Figure 12. The elaborate pattern formed by the end groups is striking, considering that only simple alkane chains with polarizable head groups are involved.

A future direction for the work is to study nonlabeled chains. Preliminary measurements indicate that the intensities are at least an order of magnitude less, but still observable. The thermodynamic properties associated with these diffraction efforts would be extremely interesting.